Journal of Nuclear Materials 205 (1993) 258–266
North-Holland

journal of nuclear materials

Amorphization kinetics of Zr_3Fe under electron irradiation

A.T. Motta [a], L.M. Howe [a] and P.R. Okamoto [b]

[a] *Reactor Materials Research Branch, AECL Research, Chalk River Laboratories, Chalk River, Ontario, Canada K0J 1J0*
[b] *Materials Science Division, Argonne National Laboratory, Argonne, IL 60439, USA*

Previous investigations using ^{40}Ar-ion bombardments have revealed that Zr_3Fe, which has an orthorhombic crystal structure, undergoes an irradiation-induced transformation from the crystalline to the amorphous state. In the present investigation, 0.9 MeV electron irradiations were performed at 28–220 K in a high-voltage electron microscope (HVEM). By measuring the onset, spread and final size of the amorphous region, factoring in the Gaussian distribution of the beam, a kinetic description of the amorphization in terms of dose, dose rate and temperature was obtained. The critical temperature for amorphization by electron irradiation was found to be ~220 K, compared with 570–625 K for ^{40}Ar-ion irradiation. Also, the dose-to-amorphization increased exponentially with temperature. Results indicated that the rate of growth of the amorphous region under the electron beam decreased with increasing temperature and the dose-to-amorphization decreased with increasing dose rate. The size of the amorphous region saturated after a given dose, the final size decreasing with increasing temperature, and it is argued that this is related to the existence of a critical dose rate, which increases with temperature, and below which no amorphization occurrs.

1. Introduction

The crystalline-to-amorphous transformation (amorphization) of intermetallic compounds induced by electron irradiation has received considerable attention since it was first reported in Fe_3B [1] and NiTi [2]. Those experiments and others that followed showed that the irradiation dose required to produce amorphization increased exponentially with temperature, so that above a critical temperature (characteristic of the material), amorphization did not occur [2–4].

Experiments initially concentrated on cataloguing compounds that were susceptible to amorphization. This led to the establishment of empirical rules to predict amorphization susceptibility, such as ionicity, melting temperature, stoichiometry, place in the phase diagram and separation in the periodic table [5]. These met with varying degrees of predictive success. One of the problems with such an approach is that since amorphization susceptibility is dependent on the irradiation conditions, the experimental data may not always be directly comparable.

Experiments in the Cu–Ti system established the fundamental role of chemical disorder in the amorphization process by showing the coincidence of the critical temperature for amorphization and that for a sharp decrease in the attainable degree of chemical disorder [3]. The role of point defects in causing amorphization rests on more indirect experimental evidence reviewed in ref. [6]. A dose rate effect has also been reported [4,7], the dose to amorphization being higher at lower dose rates.

Although there is a great deal of thermodynamic or static data available (recently reviewed in ref. [8]), only a few results have been reported that offer a kinetic description of the amorphization phenomenon [3,4,7,8]. In this study temperature-dependent kinetic data were obtained for the amorphization of Zr_3Fe. This compound was chosen because detailed experiments have been conducted on the amorphization of Zr_3Fe under ion irradiation [9,10], but no data exist for electron irradiation. Also, of particular interest is the irradiation behaviour of the various intermetallic compounds of zirconium containing Fe, Cr, Ni, Sn and Si, which are contained in the fuel cladding and pressure tubes (e.g. Zircaloy-2, Zircaloy-4 and Zr–2.5Nb alloys) of water-cooled nuclear reactors. For example, an irradiation-induced crystalline-to-amorphous transformation has been observed for $Zr(Cr,Fe)_2$ and $Zr_2(Ni,Fe)$ precipitates in Zircaloy-2 and Zircaloy-4 [11–13] and appears to be associated with the macroscopic irradiation response of these alloys in-service.

We utilize here the method used by Xu et al. [7], measuring the onset, spread and final size of the amor-

0022-3115/93/$06.00 © 1993 – Elsevier Science Publishers B.V. All rights reserved

phous region, factoring in the Gaussian distribution of the beam, to obtain the full kinetic description of amorphization in terms of dose, dose rate and temperature. The results obtained are discussed in light of previous results of Zr_3Fe amorphization by ion irradiation and of amorphization models in the literature.

2. Experimental methods

An alloy of composition $Zr_{0.8}Fe_{0.2}$ was prepared by arc melting, using Zr and Fe of 99.95 and 99.9985 at% purity, respectively. The samples were then annealed successively at 1073 K for 96 h, 1023 K for 72 h and 1000 K for 48 h. Electron-thin samples were prepared by mechanical polishing to a thickness of about 125 μm followed by electropolishing with a solution of 10% perchloric acid in methanol, kept at 223 K.

The transformed alloy that resulted from the long heat treatment consisted principally of the orthorhombic phase Zr_3Fe, with minor amounts of body-centered tetragonal Zr_2Fe and hexagonal α-Zr still present. The existence of these phases was verified by SEM and positive identification made by diffraction analysis in the TEM. All diffraction patterns obtained from the Zr_3Fe phase were consistent with the orthorhombic phase reported by Aubertin et al. [14], and compositional analysis of this phase by EDX gave the expected ratio of Zr 75% to Fe 25%.

The samples were irradiated with 0.9 MeV electrons in the HVEM at Argonne National Laboratory (ANL), at temperatures ranging from 28 to 220 K. Bright field electron micrographs and diffraction patterns from the region of interest were recorded at regular intervals during the irradiation. Considerable care was exercised to find and use markers that allowed for a consistent repositioning of the beam, after it was defocussed to take pictures. In spite of these precautions, it was inevitable that after very long irradiation times, there were some random variations of the beam position due to specimen drift and bending, minor errors in repositioning the beam, and small variations in electron current. The result of the ensemble of those effects was to "blur" the contours of the beam somewhat, making it appear slightly larger than it was.

The temperature in the cold stage holder was set to within 1 K of the desired value. The beam heating was estimated to be < 10 K, due to the low dose rates utilized. Vacuum during the experiments was better than 8×10^{-5} Pa.

The electron dose was monitored using two Faraday cups: one placed just above the specimen captures all of the beam, giving the total electron current; the other placed at the level of the screen gives an estimate of the peak value of the electron current, J_0. Assuming that the shape of the beam is Gaussian, then the electron flux is given by

$$J(r) = J_0 \exp(-r/r_0)^2, \tag{1}$$

where $J(r)$ is the electron flux [e cm^{-2} s^{-1}] and r is the distance from the center of the Gaussian. The radius r_0 is equal to $\sigma\sqrt{2}$, where σ is the standard deviation. Taking the beam radius as that which contains 95% of the beam, gives a radius of $r_0\sqrt{2}$ (i.e. 2σ).

If the beam were circular in shape, $J(r)$ could be completely determined from the ratio of the lower and upper Faraday cup currents. Since the beam is oval, the aspect ratio has to be determined as well. This was done by imposing the condition that the accumulated dose $J(r)t$ is constant throughout the edge of the amorphous oval. There is then a unique aspect ratio that makes the doses agree, for the measured radii, that being 1.266.

The actual beam size was measured from a fast exposure micrograph of the condensed beam. Its aspect ratio agreed well with the aspect ratio of the amorphous ovals, and with the calculation above.

Postirradiation examinations were conducted at Chalk River Laboratories, in a Phillips CM-30 transmission electron microscope with STEM/EDX, at 295 keV.

3. Results

At all irradiation temperatures studied, after an incubation period, an amorphous region was formed under the electron beam, which grew with increasing irradiation time. The criteria utilized for determining that an amorphous phase had been formed were the interruption of all bend contours and the disappearance of all crystalline spots from the diffraction pattern. The amorphous ring diameter corresponded to a distance of 0.247 nm.

A typical example of the development of an amorphous region is shown in fig. 1: its shape is oval, following the shape of the electron beam. Just before the formation of the well-defined amorphous region, there is a period, short compared with the total irradiation time, in which the region under the beam can be said to be partially amorphous (fig. 1c). During that period, both an amorphous ring and crystalline spots

are present, and there is a change in bright field contrast, with the lower order bend contours becoming less definite, and some of the higher order ones disappearing. The length of this period increases with increasing temperature.

The well-defined amorphous region seen in fig. 1 was seen at all irradiation temperatures up to 200 K, so the error involved in the measurement of the amorphous radius was quite small. At 220 K, however, there was a large amount of "mottling" of the region under the beam (fig. 2a), before the appearance of the amorphous oval (fig. 2c). This could be related to the formation of discrete amorphous zones as precursors of full amorphization, but a more probable explanation is that, even at this low temperature, zirconium oxide formed under the electron beam, during the prolonged irradiation. Support for this comes from the presence in the diffraction pattern from the mottled region, of sharp (microcrystalline) rings in addition to the diffuse amorphous ring (fig. 2b). The interatomic distance of the major sharp rings was 0.296 nm which is consistent with the existence of tetragonal zirconia ($a = 0.364$ nm and $c = 0.527$ nm). When present, this mottled contrast led to larger errors in the determination of the amorphous radius.

The large dimension of the amorphous oval is shown in fig. 3, as a function of irradiation time for each temperature. Each curve is completely enveloped by the preceding lower temperature curve, indicating that the amorphization kinetics slow down as the temperature increases. Both an increase in the incubation time for amorphization and a decrease in the growth rate of the amorphous zone with increasing temperature can be perceived in fig. 3.

The dose rate varies continuously with distance from the beam center, following the Gaussian shape of the beam. Since the beam profile is known from the dosimetry described in section 2, it is possible to convert the time (t)-to-amorphization to a dose-to-amorphization which is a function of r. Thus,

$$\text{dose}(r) = J(r)t. \tag{2}$$

This is done in fig. 4, where the dimensionless amorphous radius $r/r_0\sqrt{2}$ is plotted against dose, for each irradiation temperature. The dimensionless radius is used in fig. 4 because the beam was larger (by about 10 to 20%) during the irradiations at 28 and 100 K than in the others.

Since the displacement energies in Zr_3Fe are not yet well known, we did not convert the dose given in electrons per cm^2 to a dose in displacement per atom (dpa). An estimate of that conversion can be obtained by multiplying the dose in fig. 4 by the displacement cross section σ_d for 0.9 MeV electrons in Zr, but the uncertainties are large. For example, as the average threshold displacement energy varies from 25 eV to 40 eV, σ_d varies from 32×10^{-24} cm^{-2} to 0.35×10^{-24} cm^{-2} [15].

Amorphization is believed to happen when a critical dose is reached [16]. If the critical dose-to-amorphization was independent of the dose rate, then the conversion from fig. 3 to fig. 4 would yield vertical curves, indicating that, for a given temperature, the dose-to-amorphization is the same at $r = 0$ through $r = r_0\sqrt{2}$. Deviations from the straight vertical line indicate a dose-rate effect. As can be seen in fig. 4, at low temperature the dose-to-amorphization is essentially independent of dose rate. As the temperature increases, there are larger and larger deviations from the vertical, indicating the presence of an increasingly important dose-rate effect.

Fig. 4 shows that, for every temperature, at larger radii (lower dose rates) a higher dose is required to induce amorphization. Hence, the dose-to-amorphization increases with decreasing dose rate, as previously reported [4,7]. A similar dose-rate dependence for irradiation-induced amorphization of Zr_3Fe during ^{40}Ar ion irradiation has also been observed [10].

The above effect can be shown in an alternative way by making successive isodose-rate cuts in fig. 4, noting the intercept with the successive temperature curves. The dose required to reach a given radius (or the dose-to-amorphization for a given dose rate) can then be plotted as a function of temperature. As shown in fig. 5, for a given dose rate the dose-to-amorphization increases exponentially with temperature. This is the way amorphization data are usually plotted in the literature [2,4,5]. Fig. 5 shows that the critical temperature for amorphization increases with increasing dose rate, i.e., close to the critical temperature, a high dose rate makes the material amorphize whereas a low dose rate does not. Note that moving from the center of the beam along the Gaussian to a radius of 1.5 μm decreases the dose rate by approximately a factor of 2.

Fig. 4 provides a way of checking for the existence of a dose-rate effect on the critical temperature for amorphization. Three cases are possible:

(A) No dose rate effect exists, either on the dose-to-amorphization or on the critical temperature.

(B) In the absence of a dose-rate-effect on the critical temperature, the amorphous region eventually reaches the same size as the electron beam at all temperatures.

(C) Conversely, if there is such an effect, then the amorphous radius should saturate and stop growing at

the radius that corresponds to the minimum dose rate necessary for amorphization at that temperature.

The appearance of the amorphization curves in these three cases is shown schematically in fig. 6. Comparing these curves with fig. 4, it is our contention that the experimental curves follow case C. Although some of the curves appear to be still growing at the end of irradiation (cf. 220 K, and 28–150 K), the slope appears to be constantly decreasing with dose, indicating an approaching saturation, such as seen at 180 and 200 K. It should also be considered that the experimental uncertainties in this experiment, mentioned in section 2, tend to blur the tendency to saturation. For example, the sudden increase at the end of the 150 K curve is thought to be due to an involuntary misplacement of the beam center during the last leg of the irradiation. The sudden increases in beam radius observed after about 7.5×10^{22} e cm^{-2} at 180 and 200 K probably result from similar causes. Taking all those factors into consideration, the tendency towards saturation appears to be quite marked. The existence of this saturation radius means that there is a critical dose rate that increases with temperature and below which amorphization does not occur.

The present observations support previous observations of amorphization of Zr_2(Ni,Fe) [4] under electron irradiation, which also showed an increase in the critical temperature for amorphization with increasing dose rate, and is contrary to the observations by Xu et al. during amorphization of CuTi [7], which showed no dose rate effect on the critical temperature.

4. Discussion

The data presented in this paper show the amorphization kinetics in detail, thus providing an easy way of determining whether either the dose to amorphization or the critical temperature for amorphization depends on the dose rate. The analysis of the data presented above indicates that a higher damage rate increases the critical temperature and decreases the dose to amorphization. Those observations can be understood as follows.

Damage produced by irradiation is opposed by thermal annealing. The balance between the rate of damage production and the ability of the material to repair itself dictates the response of the material to irradiation. At low temperature, damage produced by irradiation remains "frozen in", with little annealing taking place. In this temperature regime, the dose to amorphization is almost independent of temperature: the damage accumulates in the lattice unchecked by thermal annealing. At a certain critical level of damage, there is a driving force to exchange the imperfect form of long-range order resulting from irradiation for a favourable local configuration of short-range order, where the bonding restrictions of chemical species and directionality are followed more closely. This explains why irradiation-induced amorphization occurs in intermetallic compounds (chemical bonding), and in Si and Ge (directionality of bonding), while in pure metals and solid solutions it does not. When the critical level is reached, the evidence is that amorphization happens catastrophically [4], possibly through a shear instability [17].

As the temperature increases, annealing processes are activated that offset the production of damage. When annealing reduces the effective damage rate without overwhelming it, a "step" appears in the dose-to-amorphization versus temperature curve, slightly increasing the dose-to-amorphization at that temperature [18,23]. The temperature at which the activated annealing process completely overwhelms damage production is the critical temperature, and amorphization is no longer possible above that temperature. It follows then that a lower damage rate is offset at a lower temperature than a higher damage rate. This implies different critical temperatures for different damage rates.

The modelling of amorphization kinetics was done in ref. [19], by solving rate equations for a fast and a slow defect in a thin foil. During the approach to steady state, which comprises all of the irradiation time (t) at low temperatures (T), the removal of the fast defect at the free surfaces of the thin foil leads to the accumulation of the slow defect according to

$$C_s \propto (G/K_{iv})^{1/4}(Gt)^{1/2}$$
$$\propto \left[G^{1/4}/\exp(-E_m^f/4kT)\right](Gt)^{1/2}, \quad (3)$$

where C_s is the concentration of the slow defect, G is the defect generation rate $J(r)\sigma_d$ (dpa s^{-1}), K_{iv} is the recombination coefficient, and E_m^f is the migration energy of the fast defect. The above equation explains both the dose rate effect and the temperature effect. For a given dose, Gt, the concentration of the slow defect is higher when G is higher and when T is lower. The dose rate effect can also be explained by a chemical disordering approach, as pointed out by Basu et al. [20], but no simple expression such as eq. (3) exists to express that fact.

Comparing the results obtained here under electron irradiation, with the results previously obtained under

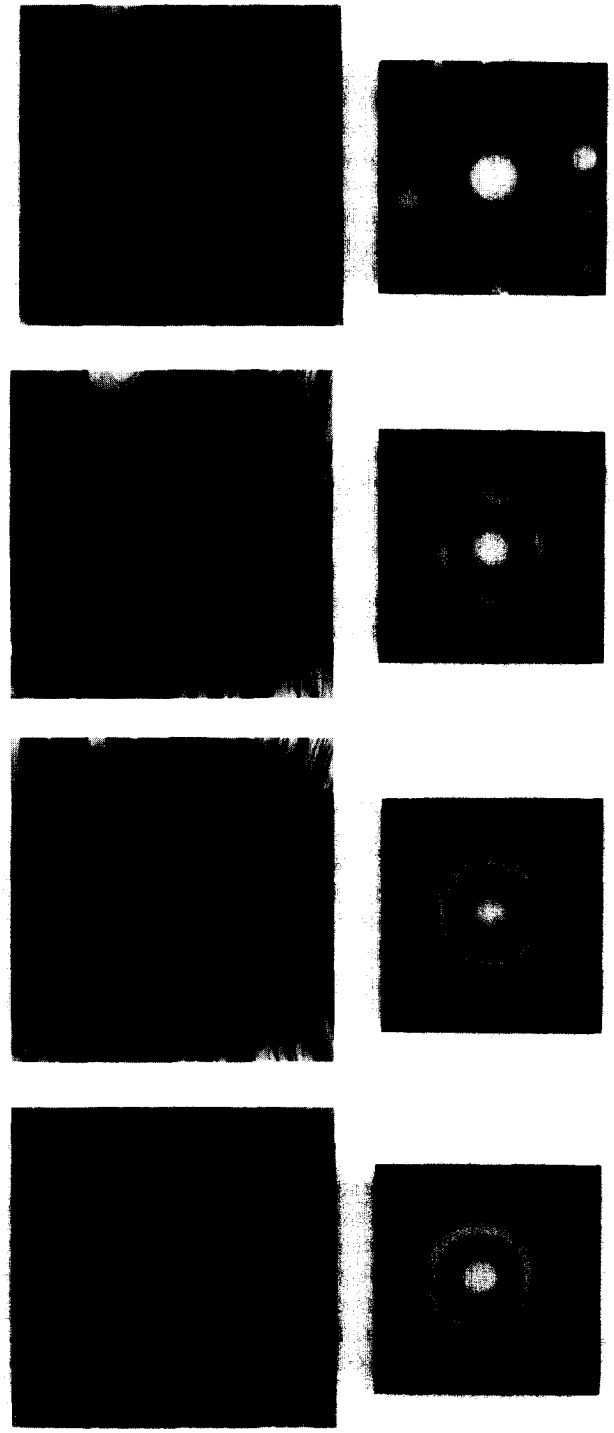

Fig. 1. Bright field electron micrographs and corresponding diffraction patterns for Zr_3Fe irradiated at 100 K with 0.9 MeV electrons, for the following accumulated times: (a,b) 0 s, (c,d) 60 s, (e,f) 302 s, and (g,h) 1262 s.

^{40}Ar-ion irradiation [9,10], the most obvious difference is that the critical temperature for amorphization of Zr_3Fe during ion irradiation is much higher than that under electron irradiation. Previously published results indicated the presence of several different temperature regimes: a dose of 5×10^{15} Ar-ions cm^{-2} (0.5 to 1.5 MeV) caused complete amorphization at 110 K, partial amorphization at 160 K, and no amorphization at 623 K. Since after a dose of 1×10^{15} ions cm^{-2} discrete amorphous regions were observed at 473 K, the critical temperature lies between 473 and 623 K. Additional information was recently obtained with in-situ ion irradiations of Zr_3Fe at ANL [21], which showed amorphization starting to occur at 572 K, after a dose of 5×10^{15} Ar-ions cm^{-2} (350 keV), so the critical temperature for ^{40}Ar-ion irradiation is bracketed between 572 and 623 K.

By contrast, the present results indicate that the critical temperature for amorphization under electron irradiation is slightly higher than 220 K, a difference of more than 300 K. Similar differences between the critical temperatures of amorphization induced by ion and electron irradiation have also been found in CuTi [22] and in intermetallic precipitates in Zircaloy [23]. Also Zr_3Al, although easily amorphized by ion irradiation [24], was recently found to amorphize under electron irradiation, but only below 15 K [25]. The difference is due to the fact that ion irradiation produces displacement cascades, while electron irradiation produces isolated Frenkel pairs. Within the cascades the density of the damage is quite high and amorphization can then occur either directly in the cascade or upon cascade superposition. For example, discrete damaged regions, believed to be amorphous in nature, have been observed in Zr_3Fe irradiated with 0.5–1.5 MeV ^{40}Ar ions and with 15–120 keV ^{209}Bi ions [10,26].

Thus, while the overall damage rate of electron irradiation can be up to two orders of magnitude higher than ion irradiation, the fact that the damage is homogeneously distributed throughout the material makes it easier to anneal, so the upper temperature limit of amorphization is lower than that for ions.

The increase in dose-to-amorphization between 150 and 220 K under electron irradiation corresponds well to the change in amorphization regime occurring between 110 and 160 K under ^{40}Ar-ion irradiation. At 110 K and below, the dose-to-amorphization during ^{40}Ar-ion irradiation is smaller than at 160 K. Below 160 K, the regions in between cascades do not get annealed before the next cascade hits. At 160 K and above, some type of defect becomes mobile. The resulting defect annihilation produces a less damaged outer region of

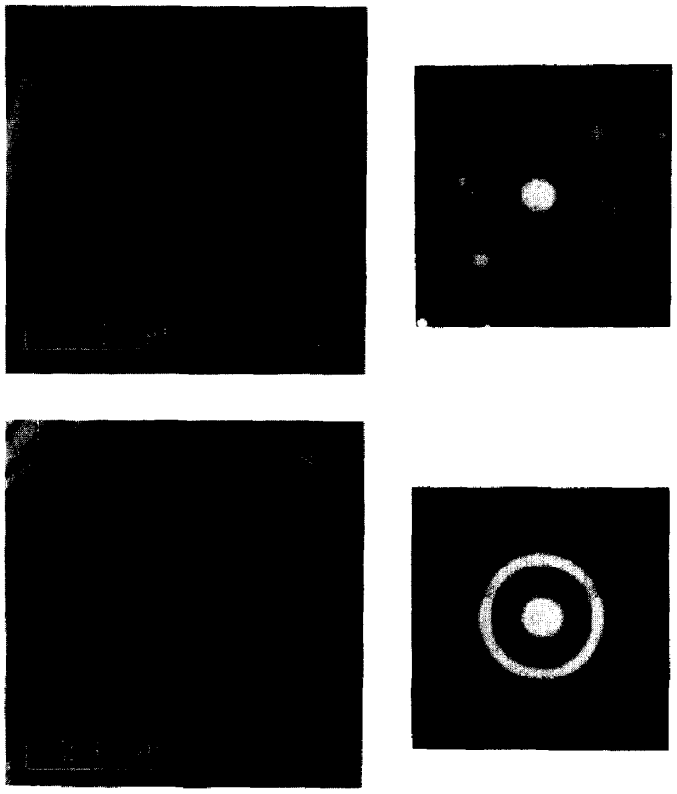

Fig. 2. Bright field electron micrographs and corresponding diffraction patterns for Zr_3Fe irradiated with 0.9 MeV electrons at 220 K for 3497 s (a,b) and 9448 s (c,d).

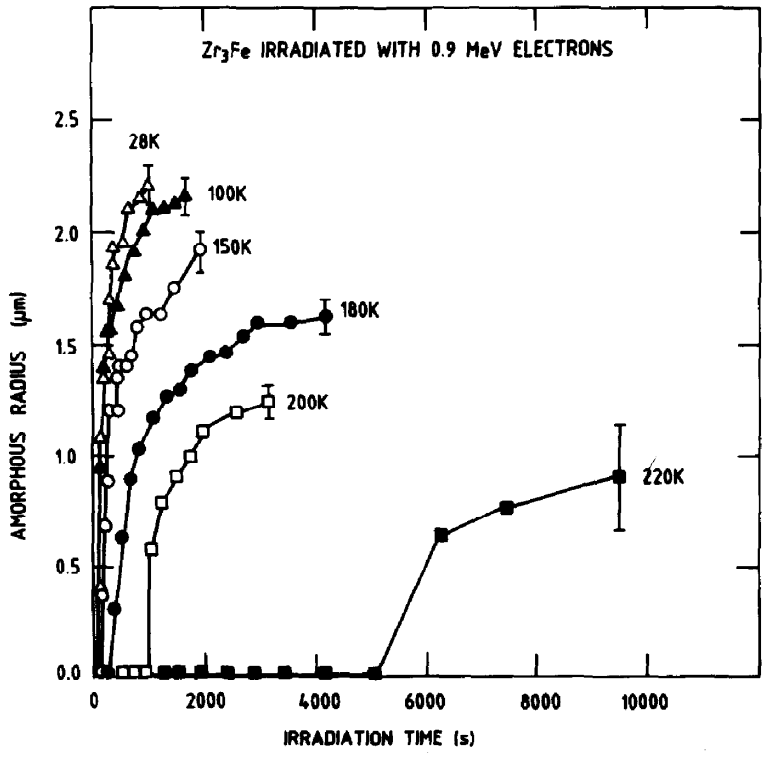

Fig. 3. Large dimension of the amorphous oval as a function of irradiation time for each temperature.

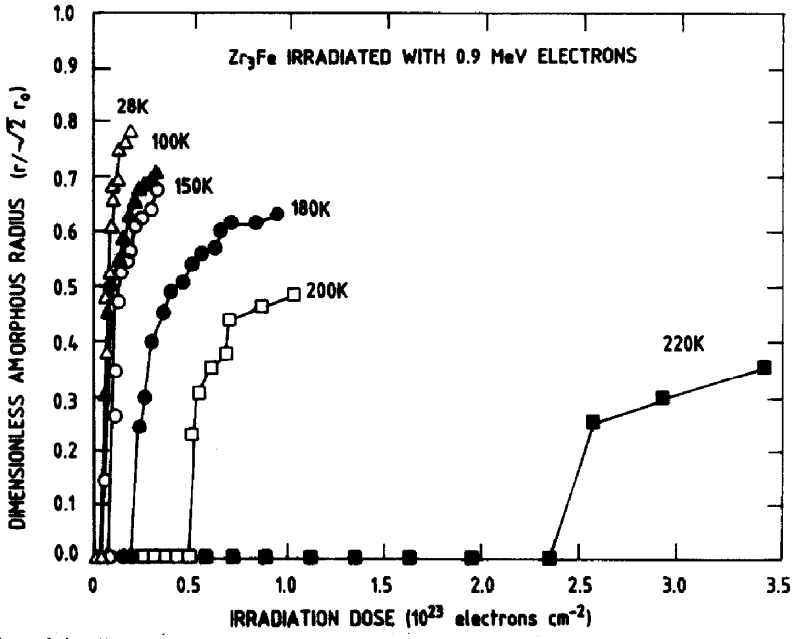

Fig. 4. Variation of the dimensionless amorphous radius with electron-irradiation dose at various temperatures.

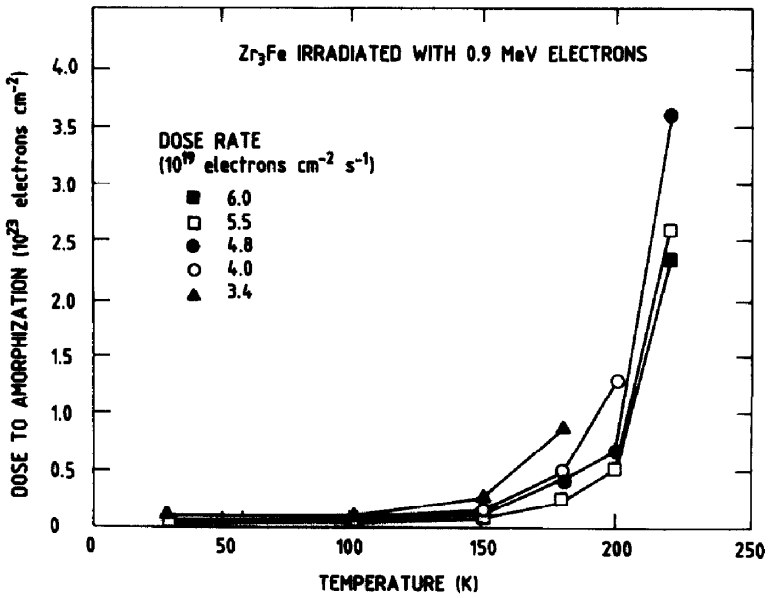

Fig. 5. Dose-to-amorphization versus irradiation temperature for each dose rate.

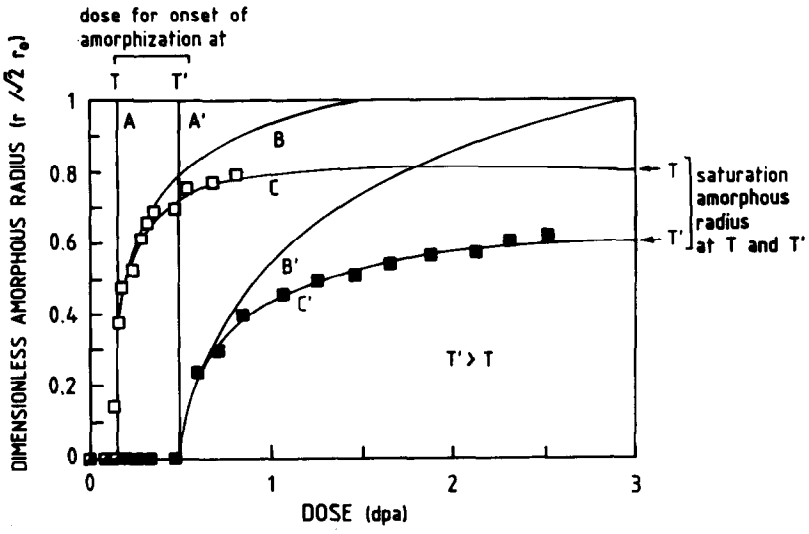

Fig. 6. Dimensionless amorphous radius versus electron dose for the different cases (A, B and C) outlined in the text. Experimental points at 28 K (T) and 180 K (T') are included for comparison.

the cascade, leaving a smaller heavily damaged core, thus requiring more extensive coverage of the material for complete amorphization.

5. Conclusions

The kinetics of amorphization of Zr_3Fe induced by electron irradiation have been studied at a range of temperatures between 28 and 220 K. The dose-to-amorphization increases exponentially with temperature. The critical temperature for amorphization is approximately 220 K, whereas for Ar-ion irradiation it is higher than 570 K.

Results indicate that the rate of growth of the amorphous region under the beam decreases with increasing temperature, in a monotonic fashion. It is shown that a dose rate effect exists, and that the dose-to-amorphization decreases for increasing dose rate.

The size of the amorphous region saturates after a given dose, the final size decreasing with increasing temperature. It is argued that this is related to the existence of a critical dose rate, which increases with temperature, below which no amorphization occurs.

Acknowledgements

Thanks are due to D. Phillips and H.H. Plattner at Chalk River Laboratories, for sample preparation and technical assistance, and to the staff of the dual HVEM/ion facility at Argonne National Laboratory, E. Ryan, S. Ockers and L. Funk, for their assistance in the irradiations.

This research project is funded through a Candu Owners Group (COG) contract. We wish to thank the COG Working Party 32 Committee for their financial support and interest in the program.

References

[1] A. Mogro-Campero, E.L. Hall, J.L. Walter and A.J. Ratkwoski, in Metastable Materials Formation by Ion Implantation, eds. S.T. Picraux and W.J. Choike (Elsevier, Lausanne, 1982) p. 203.

[2] G. Thomas, H. Mori, H. Fujita and R. Sinclair, Scripta Metall. 16 (1982) 589.

[3] D.E. Luzzi and M. Meshii, Scripta Metall. 20 (1986) 943.

[4] D.E. Luzzi, H. Mori, H. Fujita and M. Meshii, Acta Metall. 34 (1986) 629.

[5] A.T. Motta, D.R. Olander and A.J. Machiels, Proc. 14th Int. Symp. on the Effects of Irradiation on Materials, Andover, 1988, eds. N.H. Packan, R.E. Stoller and A.S. Kumar, ASTM-STP 1046 (1989) p. 457.

[6] A.T. Motta and C. Lemaignan, in Ordering and Disordering in Alloys, ed. A.R. Yavari (Elsevier, New York, 1992) p. 255.

[7] G. Xu, J. Koike, P.R. Okamoto and M. Meshii, Proc. 47th EMSA Meeting, 1989, p. 658.

[8] P.R. Okamoto and M. Meshii, in Science of Advanced Materials, eds. H. Wiedersich and M. Meshii (ASM, 1992) p. 33.

[9] L.M. Howe, D.P. McCooeye, M.H. Rainville, J.D. Bonnett and D. Phillips, Nucl. Inst. and Meth. B59 (1991) 884.
[10] L.M. Howe, M.H. Rainville and D. Phillips, in Phase Formation and Modification by Beam–Solid Interactions, eds. G.S. Was, L.E. Rehn and D.M. Follstaedt, Mater. Res. Soc. Symp. Proc. 235 (1992) 461.
[11] W.J.S. Yang, R.P. Tucker, B. Cheng and R.B. Adamson, J. Nucl. Mater. 138 (1986) 185.
[12] M. Griffiths, J. Nucl. Mater. 159 (1988) 190.
[13] F. Lefebvre and C. Lemaignan, J. Nucl. Mater. 165 (1989) 122.
[14] F. Aubertin, U. Gonser, S.J. Campbell and H.-G. Wagner, Z. Metallk. 76 (1985) 237.
[15] O.S. Oen, ORNL Report 4897 (1973).
[16] M.L. Swanson, J.R. Parsons and C.W. Hoelke, Radiat. Eff. 9 (1971) 249.
[17] L.E. Rehn, P.R. Okamoto, J. Pearson, R. Bhadra and M. Grimsditch, Phys. Rev. Lett. 59 (1987) 2987.
[18] J. Koike, D.E. Luzzi, M. Meshi and P.R. Okamoto, Mater. Res. Soc. Symp. Proc. 74 (1987) 425.
[19] A.T. Motta and D.R. Olander, Acta Metall. and Mater. 38 (11) (1990) 2175.
[20] S.N. Basu, T.E. Mitchell and M. Nastasi, J. Appl. Phys. 69 (1991) 3165.
[21] L.M. Howe, A.T. Motta and P.R. Okamoto, unpublished data.
[22] J. Koike, P.R. Okamoto, L.E. Rehn and M. Meshii, J. Mater. Res. 4 (1989) 1143.
[23] A.T. Motta, L.M. Howe and P.R. Okamoto, Beam–Solid Interactions, vol. 279, eds. M.A. Nastasi, N. Herbots, L.R. Harriott and R.S. Averbach, Proc. A of MRS Society, Fall Meeting, Boston, MA, November 30–December 4, 1992, in press.
[24] L.M. Howe and M.H. Rainville, J. Nuc. Mater. 68 (1977) 215.
[25] J. Koike, P.R. Okamoto, L.E. Rehn and M. Meshii, Metall. Trans. 21A (1990) 1799.
[26] L.M. Howe, M.H. Rainville, D. Phillips, H.H. Plattner and J.D. Bonnett, Proc. 8th Int. Conf. on Ion Beam Modifications of Materials, Heidelberg, Germany, September 7–11, 1992, in press.